

Capillary number correlations for two-phase flow in porous media

R. Hilfer

ICP, Universität Stuttgart, 70569 Stuttgart, Germany

 (Received 20 August 2020; accepted 8 October 2020; published 4 November 2020)

Relative permeabilities and capillary number correlations are widely used for quantitative estimates of enhanced water flood performance in porous media. They enter as essential parameters into reservoir simulations. Experimental capillary number correlations for seven different reservoir rocks and 21 pairs of wetting and nonwetting fluids are analyzed. The analysis introduces generalized local macroscopic capillary number correlations. It eliminates shortcomings of conventional capillary number correlations. Surprisingly, the use of capillary number correlations on reservoir scales may become inconsistent in the sense that the limits of applicability of the underlying generalized Darcy law are violated. The results show that local macroscopic capillary number correlations can distinguish between rock types. The experimental correlations are ordered systematically using a three-parameter fit function combined with a novel fluid pair based figure of merit.

DOI: [10.1103/PhysRevE.102.053103](https://doi.org/10.1103/PhysRevE.102.053103)

I. INTRODUCTION

An unanswered challenge for theoretical physics has been to improve those mathematical models for immiscible displacement of oil $\circ \subset \mathfrak{s}$ and water $\mathfrak{w} \subset \mathfrak{s}$ inside a porous sample $\mathfrak{s} \subset \mathbb{R}^3$ that are universally accepted and applied in hydrology and petroleum engineering [1–7]. Diverse subfields of theoretical physics have sprung or benefited from this challenge, most notably percolation theory [8–11], but the problem remains unsolved and of active theoretical and applied interest [12–15].

Mathematical models for two-phase immiscible displacement are based on a generalization of Darcy’s law for single-phase flow through a rigid medium. A rigid porous sample $\mathfrak{s} \subset \mathbb{R}^3$ is represented in Darcy’s model as the union $\mathfrak{s} = \mathfrak{p} \cup \mathfrak{m}$ of a pore space \mathfrak{p} and a matrix \mathfrak{m} , both closed subsets of \mathfrak{s} . Its internal boundary, denoted $\partial \mathfrak{m} = \partial \mathfrak{p} = \mathfrak{p} \cap \mathfrak{m}$, is assumed to be fixed (rigid). Outlet and inlet of the pore space \mathfrak{p} are assumed to be percolating, i.e., connected by a path contained within the pore space. Recall that Darcy’s law for single-phase fluid flow through a sample \mathfrak{s} Kas (Ref. [5], p. 74 and Ref. [16], p. 79) postulates

$$\mathbf{v}(\mathfrak{s}, \mathfrak{p}) = \phi(\mathfrak{p}) \mathbf{v} = \frac{k(\mathfrak{p})}{\mu} \frac{\Delta P(\mathfrak{s})}{L(\mathfrak{s})}, \quad (1)$$

where $\mathbf{v}(\mathfrak{s}, \mathfrak{p})$ is the magnitude of the (superficial) Darcy velocity, $v = |\mathbf{v}|$ is the magnitude of the phase velocity of the (interstitial) fluid, μ is the viscosity of the fluid, $\Delta P(\mathfrak{s})$ is the macroscopic pressure drop across the sample, $L(\mathfrak{s})$ is the sample size, $\phi(\mathfrak{p})$ is the porosity, and $k(\mathfrak{p})$ is the absolute permeability of \mathfrak{p} . Equation (1) holds for sufficiently slow unidirectional flow. Matrix \mathfrak{m} , pore space \mathfrak{p} , and sample \mathfrak{s} are assumed throughout to be elements of the so called convex ring \mathcal{R} [17], defined as the set of all finite unions of compact convex subsets of \mathbb{R}^3 .

Darcy’s law for a mixture of two immiscible fluids is not based on mean-field-type volume averaging assumptions, but on the idea of “freezing out phases” [5,18]. Early on it was noticed that the presence of the second phase not only reduces the permeability to the first, but also decreases the permeability to the mixture (Ref. [5], p. 215). It is this observation that forms the constitutive model of two-phase flow in porous media [see Eq. (6) below].

Generalizing from one-phase flow to two immiscible fluids, such as oil \circ and water \mathfrak{w} , the pore space is decomposed as $\mathfrak{p} = \circ \cup \mathfrak{w}$ into the two phases present. Let $\text{in}(\mathfrak{a})$, the interior of a set $\mathfrak{a} \in \mathcal{R}$, be defined as the union of all open sets contained in the set \mathfrak{w} . One assumes that $\text{in}(\mathfrak{w}) \cap \text{in}(\circ) = \emptyset$ holds. Relevant geometric quantities for porous media are the functionals $\phi : \mathcal{R} \rightarrow [0, 1]$ and $S : \mathcal{R} \rightarrow [0, 1]$ defined by $\phi(\mathfrak{w}) := |\mathfrak{w}|/|\mathfrak{s}|$ and $S(\mathfrak{w}) := |\mathfrak{w}|/|\mathfrak{p}|$, where the “absolute value of a set” $|\mathfrak{w}|$ means the volume of the set $\mathfrak{w} \subset \mathbb{R}^3$. If the index notation $\phi(\mathfrak{w}) = \phi_{\mathfrak{w}}$ and $S(\mathfrak{w}) = S_{\mathfrak{w}}$ is used, then this yields the relations

$$\phi_{\mathfrak{w}} = \phi_{\mathfrak{p}} S_{\mathfrak{w}}, \quad (2a)$$

$$\phi_{\circ} = \phi_{\mathfrak{p}} S_{\circ}, \quad (2b)$$

$$\phi_{\mathfrak{p}} = \phi_{\mathfrak{w}} + \phi_{\circ}, \quad (2c)$$

$$1 = S_{\mathfrak{w}} + S_{\circ}, \quad (2d)$$

for volume fractions in standard notation. A stationary two-phase flow at constant saturation $S = S_{\mathfrak{w}} = 1 - S_{\circ}$ and constant phase velocities $\mathbf{v}_{\mathfrak{w}}$ and \mathbf{v}_{\circ} becomes a one-phase flow in two important special cases, namely

$$|\mathbf{v}_{\mathfrak{w}}| = v_{\mathfrak{w}} \quad \text{and} \quad |\mathbf{v}_{\circ}| = 0, \quad (3a)$$

$$|\mathbf{v}_{\mathfrak{w}}| = 0 \quad \text{and} \quad |\mathbf{v}_{\circ}| = v_{\circ}, \quad (3b)$$

obtained from mentally “freezing” one of the two fluids, i.e., by in turn setting the second velocity to zero. “Mentally freezing” a fluid means to mentally merge the frozen fluid with

the rigid matrix, and hence Darcy's law for single-phase flow, Eq. (1), applies to the nonfrozen fluid.

The "freezing" conditions in Eqs. (3a) and (3b) both express the physical idea that for sufficiently small flow rates $v \rightarrow 0$ the water-oil interface is kept fixed by capillary forces. For larger velocities, viscous stresses start to mobilize these interfaces. Thus, Eqs. (3a) and (3b) hold true only if

$$(\text{viscous forces}) \ll (\text{capillary forces}) \quad (4)$$

holds locally in a representative elementary volume (REV) for the local velocities v_w, v_o . The reader is referred to [19] for a discussion of scaling limits and the conceptual basis of REV's. The inequality (4) establishes a connection between the freezing condition (3) and capillary numbers defined as the ratio of viscous to capillary forces on the scale of representative elementary volumes.

II. OBJECTIVES

The objective of this work is to report quantitative experimental estimates for the balance of viscous and capillary forces in sandstones and limestone. The estimates differ dramatically (by several decades) from currently employed estimates.

Currently, capillary forces inside of porous media are usually quantified by the interfacial tension σ between oil and water as it is measured outside of porous media. In the great majority of contemporary research articles (see, e.g., Ref. [20], p. 4834) and textbooks (see, e.g., Ref. [7], p. 33), the microscopic capillary number

$$\text{miCa}_i = \frac{\mu_i v_i}{\sigma} = \frac{(\text{microscale viscous forces in } i)}{(\text{microscale capillary forces})} \quad (5)$$

is used to estimate the viscous to capillary force ratio. Here $i = w, o$ is the displacing fluid and σ is the interfacial tension between the two fluids. Although it is widely known and appreciated that the mobilization of residual oil by water floods depends not only upon flow velocity, viscosity, and interfacial tension, but also on the geometrical structure and wetting properties of the medium, the misleading force balance in Eq. (5) is invariably invoked to quantify the force balance.

The shortcomings of the force balance Eq. (5) have been repaired by using the generalized Darcy law [21]. However, these theoretical results have not been convincingly tested experimentally in the available literature. It is the purpose of this paper to fill this gap. Conclusive experimental evidence for the theoretical results and predictions of macroscopic capillary numbers will be given below. In addition, this work introduces a generalization that might be called "local macroscopic capillary numbers."

III. MATHEMATICAL MODEL

The universally accepted and applied mathematical model for two-phase flow in porous media is based on two constitutive assumptions, namely the generalized Darcy law and the capillary pressure-saturation relation. The generalized Darcy model is inspired by the idea of "freezing" oil or water in (3). It postulates the Darcy law (1) twice, once for water with

frozen oil, case (3a), and once for oil with frozen water, case (3b), as

$$\mathbf{v}_w = \phi_w v_w = \frac{k(w) \Delta P_w(\mathfrak{s})}{\mu_w L(\mathfrak{s})}, \quad (6a)$$

$$\mathbf{v}_o = \phi_o v_o = \frac{k(o) \Delta P_o(\mathfrak{s})}{\mu_o L(\mathfrak{s})}, \quad (6b)$$

where $k : \mathcal{R} \rightarrow \mathbb{R}$ is the permeability functional and $\Delta P_w, \Delta P_o$ are the macroscopic viscous pressure drops in the flowing phases over the macroscopic sample size L .

Consider now a path $[t_0, t_1] \ni t \mapsto \mathbf{w}(t) \in \mathcal{R}$ of frozen fluid configurations in \mathcal{R} with $t_0, t_1 \in \mathbb{R}$. Every such path determines two graphs,

$$\mathbf{G}_w = \{(k(\mathbf{w}(t)), S(\mathbf{w}(t))) | t \in [t_0, t_1]\}, \quad (7a)$$

$$\mathbf{G}_o = \{(k(\mathfrak{p} \setminus \mathbf{w}(t)), S(\mathfrak{p} \setminus \mathbf{w}(t))) | t \in [t_0, t_1]\} \quad (7b)$$

in the (k, S) -plane. It is often the case and commonly assumed that these two graphs are the graphs of two functions

$$k_{\mathbf{G}_i} = k_i : [0, 1] \rightarrow \mathbb{R}, \quad (8)$$

$$S_i \mapsto k_i(S_i) = k k_i^r(S_i)$$

of saturation, where $i = w, o$. The relative permeability functions $k_i^r : [0, 1] \rightarrow [0, 1]$ are defined by factoring out the absolute permeability k from the effective permeabilities k_i as $k_i(S_i) = k k_i^r(S_i)$. The dependence of k_i^r on the path and the resulting graphs \mathbf{G}_i is often notationally suppressed when hysteresis between drainage and imbibition is neglected.

It is common to assume the existence of an irreducible water saturation $0 < S_{wi}$ with $S_{wi} \not\approx 1$ such that

$$k_w^r(S_{wi}) = 0 \quad (9)$$

for all $S \leq S_{wi}$ and a residual oil saturation $0 < S_{or}$ with $S_{or} \not\approx 1$ such that

$$k_o^r(1 - S_{or}) = 0 \quad (10)$$

for all $S \geq 1 - S_{or}$. These equations define S_{wi} and S_{or} .

The relative permeability functions $k_i^r(S)$ are assumed to be non-negative and monotone functions of saturation. An example is the power-law form

$$k_w^r(S) = k_w^{re} S_e^\gamma, \quad (11a)$$

$$k_o^r(S) = k_o^{re} (1 - S_e)^\delta \quad (11b)$$

with end points k_w^{re}, k_o^{re} and $\gamma, \delta > 0$ (Ref. [22], p. 27). Here

$$S_e(S) = \frac{S - S_{wi}}{1 - S_{or} - S_{wi}} \quad (12)$$

is the effective saturation.

The existence of a curved water-oil interface $\partial_{w/o} = w \cap o$ at the pore scale results in a pressure difference on the Darcy scale between the pressures P_o in the nonwetting phase and P_w in the wetting phase. The difference

$$P_o - P_w = P_c(o, w) = P_c(\mathfrak{p} \setminus w, w) \quad (13)$$

is the capillary pressure functional $P_c : \mathcal{R} \times \mathcal{R} \rightarrow \mathbb{R}$. It depends on the fluid configurations, on interfacial tensions, on the geometry of the matrix and its wetting properties, and perhaps other factors. Exchanging o with w in Eq. (13) shows

TABLE I. Rock sample descriptions from Ref. [25] (Table 1). Columns G , S_{ai} , and P_d are the parameters from Ref. [24] (Table 1) for the mercury-air primary drainage capillary pressure as given by Eq. (18). The irreducible air saturation is obtained as $S_{ai} = 1 - [(V_b)_{P_\infty} / \phi]$, where $(V_b)_{P_\infty}$ is the fractional bulk volume occupied at infinite pressure. The column P_d^{th} gives the theoretical displacement pressure $P_d^{th} = \gamma \sqrt{\phi/k}$ with ϕ and k from the first and second column and the mercury-air interfacial tension $\gamma \approx 0.486$ N/m.

No.	Description	ϕ	k (10^{-12} m ²)	G	S_{ai}	P_d^{exp} (Pa)	P_d^{th} (Pa)	P_d^{th}/P_d^{exp}
796	Gallup sandstone	0.267	1.135	0.06	0.026	54469	235725	4.33
798	Dalton sandstone	0.276	0.483	0.10	0.047	48263	367160	7.61
799	Dalton sandstone	0.284	0.138	0.10	0.201	81358	696779	8.56
878	Paluxy sandstone	0.268	1.836	0.05	0.034	40679	185699	4.56
879	Bandera sandstone	0.226	0.032	0.30	0.181	159269	1300107	8.16
880	Berea sandstone	0.209	0.306	0.20	0.081	41369	401691	9.71
881	Indiana limestone	0.200	0.026	1.10	0.260	39990	1356838	33.93

that $P_c(\circlearrowleft, w) = -P_c(w, \circlearrowleft)$. Every path of frozen fluid configurations now gives rise to a single graph

$$\mathbf{G} = \{(P_c(p \setminus w(t), w(t)), S(w(t))) | t \in [t_0, t_1]\} \quad (14)$$

in the (P_c, S) -plane. This graph is assumed to be the graph of the capillary pressure function

$$P_c : [0, 1] \rightarrow \mathbb{R}, \quad (15)$$

$$S \mapsto P_c(S),$$

denoted again by the same symbol. Its dependence on the path or process is suppressed as in the case of k_i^r . The capillary pressure is factorized as

$$P_c(S) = P_b \widehat{P}_c(S), \quad (16)$$

where the parameter P_b is a typical capillary pressure. It can be chosen in various ways. Here the midpoint value

$$P_b = P_c \left(\frac{S_{wi} + 1 - S_{or}}{2} \right) \quad (17)$$

will be used in analogy with Ref. [23] [Eq. (18)]. The functional form

$$P_c(S) = P_d 10^{-G/\lg[1-S_c(S)]} \quad (18)$$

from Ref. [24] [Eq. (3)] is widely used for mercury-air drainage in mercury porosimetry. The pressure P_d in Eq. (18) is the mercury-air extrapolated displacement pressure [Ref. [24], Eq. (3)]. The symbol $\lg = \log_{10}$ is the logarithm with base 10, and $G > 0$ is the pore geometrical factor. Air is the wetting fluid, and mercury is the nonwetting fluid in mercury porosimetry. Hence $S_{wi} = S_{ai}$ is the irreducible air saturation in Eq. (12). The residual nonwetting phase saturation S_{or} is assumed to be zero in [24].

IV. EXPERIMENTS

Flow experiments for six different sandstones and one limestone were reported in [25]. The rock properties are listed in Table I. The cores used in the flow experiments all had a diameter of 2.54 cm and lengths from 5.08 cm up to 8.89 cm. All samples were strongly water wet.

Mercury porosimetry was performed on all cores. The air-mercury capillary pressure was fitted using Eq. (18). The parameters for these fits are listed in Table I and the resulting primary drainage curves for all samples are displayed

in Fig. 1. Note the large difference in the pore geometrical factor G between the sandstones (samples 796–880) and the limestone (sample 881).

A central objective of the experiments was to investigate the influence of viscosity ratio and interfacial tension on residual oil saturation. Residual oil saturation after a water flood can be considerably reduced if the water viscosity is increased or its interfacial tension with oil is lowered. All in all, 21 pairs of fluids were used in the experiments. The properties of the fluids are listed in Table II.

The experimental procedure starts from a water flooded sample at water saturation $S_w = 1 - S_{or}^{wf}$ where S_{or}^{wf} is the residual oil saturation after a previous water flood. In [25] the notation S_{or} is used for S_{or}^{wf} . Here the notation S_{or}^{wf} is preferred to emphasize that $S_{or}^{wf} \neq S_{or}$, where S_{or} is defined in Eq. (10). An experiment is carried out in three steps:

(1) Drainage with standard mineral oil:

(i) Drain the water from a previously water flooded sample (at $S_w = 1 - S_{or}^{wf}$) using a refined white mineral oil with a viscosity of $\mu_o = 0.3$ Poise.

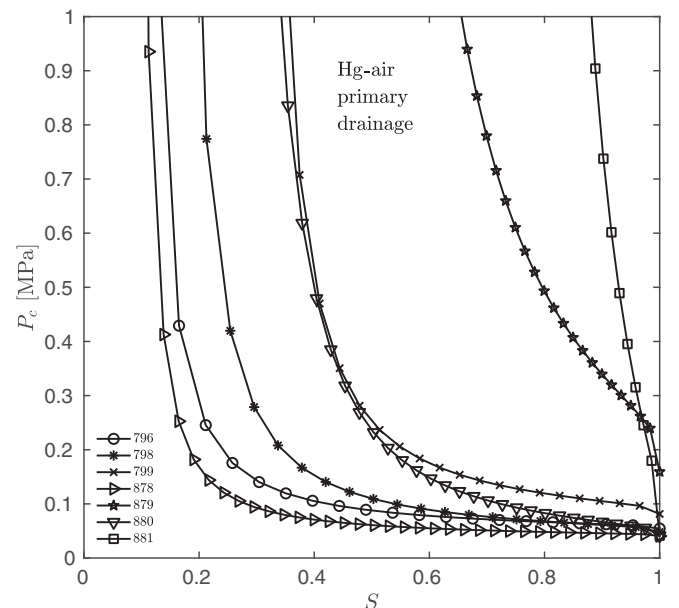


FIG. 1. Capillary pressure for the samples listed in Table I. Parameters for Eq. (18) from (Ref. [25], Table 3).

TABLE II. Table entries give the interfacial tensions $\sigma = \sigma_{w\circ}$ in units of 10^{-3} N/m for pairs of fluids with viscosity in units of 10^{-3} Pa s given as row and line headers.

Viscosities	$\mu_w = 0.94$	$\mu_w = 3.15$	$\mu_w = 9.0$	$\mu_w = 32.3$
$\mu_\circ = 0.401$	50.0	37.4	33.7	32.0
$\mu_\circ = 1.23$				5.0
$\mu_\circ = 1.26$	50.0	35.4	32.8	31.3
$\mu_\circ = 1.5$			1.8	
$\mu_\circ = 3.0$	50.0	37.0	35.5	32.8
$\mu_\circ = 9.0$	50.0	37.0	36.3	31.5
$\mu_\circ = 30.5$	50.0	38.6	34.5	33.1

(ii) Measure the volume of water displaced and determine the initial oil saturation S_{oi} listed in Ref. [25] (Table 3, column 5).

(2) Exchange standard mineral oil with test oil:

(i) Replace the white mineral oil with the test oil of interest by flowing five to ten pore volumes of the test oil through the sample.

(ii) Measure k_o^r in the final steady state.

(3) Enhanced water flood with test water (Imbibition):

(i) Perform the water flood injecting the test water of prescribed viscosity and interfacial tension into the test oil filled sample.

(ii) Monitor the produced volume of test oil and determine the value of S_{or}^{wf} in Ref. [25] (Table 3, column 6) for this experiment.

(iii) Flow five to ten pore volumes of test water through the sample.

(iv) Measure k_w^r [listed in Ref. [25] (Table 3, column 7)] in the final steady state.

The preparatory steps (1) and (2) ensure that all water floods start from a fluid configuration where the oil phase is continuous and in contact with the flooding water.

V. CAPILLARY NUMBER CORRELATIONS

The experiments in [25] are analyzed by introducing what might be called a method of “local macroscopic force balance” or “local macroscopic capillary number correlation.” “Local” here refers to the necessity of averaging over a representative elementary volume for all the quantities appearing in Eqs. (6) and (13). The qualitative condition (4) of validity and applicability of Eqs. (6) and (13) can be quantified locally by writing

$$\frac{|(\text{local macroscopic viscous pressure drop})|}{|(\text{local capillary pressure difference})|} \ll 1 \quad (19)$$

for each phase. Thus the local macroscopic capillary number is defined as

$$\begin{aligned} \text{lmCa}_i &:= \frac{|(\text{viscous pressure drop in } i)|}{|(\text{capillary pressure difference})|}, \\ &= \frac{|\Delta P_i|}{|P_\circ - P_w|}, \\ &= \frac{\mu_i v_i L}{k^{(i)} |P_c(\mathbb{P} \setminus i, i)|} \end{aligned} \quad (20)$$

for phase $i = w, \circ$. Here the constitutive equations (6) and (13) were used.

Going from the configuration-dependent functionals $k^r(i)$ and $P_c(\circ, w)$ to saturation-dependent functions $k_i^r(S)$ and $P_c(S)$ under the assumptions discussed above, the local macroscopic capillary number can be expressed as

$$\text{lmCa}_i = \frac{\mu_i \phi S_i v_i L}{k k_i^r(S_i) P_b |\widehat{P}_c(S_i)|}, \quad (21)$$

where $i = w, \circ$ and Eqs. (8) and (16) were used. This can be rewritten as

$$\text{lmCa}_i = \frac{\text{maCa}_i S_i}{k_i^r(S_i) |\widehat{P}_c(S_i)|}, \quad (22)$$

where

$$\text{maCa}_i = \frac{\mu_i \phi v_i L}{k P_b} \quad (23)$$

are the macroscopic capillary numbers introduced in [21,26].

Given that the macroscopic capillary forces are quantified according to Eq. (17) by the capillary pressure at midpoint saturation it would seem that also the macroscopic viscous forces should be quantified at midpoint saturation. That suggests to introduce the global macroscopic capillary number as

$$\text{gmCa}_i = \frac{\mu_i \phi v_i L}{k k_{bi}^r P_b}, \quad (24)$$

where

$$k_{bi}^r = k_i^r \left(\frac{S_{wi} + 1 - S_{or}}{2} \right) \quad (25)$$

is the relative permeability evaluated at the saturation midpoint. It is expected that $\text{lmCa}_i < \text{gmCa}_i$ holds.

The experimental local macroscopic capillary number correlation can be fitted with the fit function

$$S_{or}^{wf}(\text{lmCa}) = S_{or}^{pl} (1 - [1 + (A \text{lmCa})^{-\alpha}]^{-\beta}) \quad (26)$$

with parameters $S_{or}^{pl} = S_{or}^{wf}(0) \in [0, 1]$, $A > 0$, and $\alpha, \beta > 0$. The parameters are expected to depend on the viscosity ratio and the interfacial tension between the two fluids.

It is experimentally known that S_{or}^{wf} tends to be small when the viscosity ratio μ_w/μ_\circ is large or the interfacial tension is low. This suggests to introduce a figure of merit defined as

$$H = \frac{\sigma \mu_\circ}{\mu_w^2} \quad (27)$$

for a given pair of fluids. It is obtained by dividing σ/μ_w with the viscosity ratio μ_w/μ_\circ . The residual oil saturation is expected to be small when the figure of merit is small. Note that σ/μ_w is the characteristic velocity v^* such that $\text{miCa} = v/v^*$. For $v < v^*$, the capillary forces dominate, while for $v > v^*$ viscous friction disrupts and finally destroys the coherence of the fluid-fluid interface.

VI. RESULTS

A. Microscopic CNCs

Ordinary traditional microscopic capillary number correlations $S_{or}^{wf}(\text{miCa})$ (also known as capillary desaturation

curves) were published in [25]. The most obvious shortcoming of the dimensionless group $miCa$ (on the abscissa of Ref. [25], Fig. 4) and $F := miCa (\mu_w/\mu_o)^{0.4}$ (on the abscissa of Ref. [25], Figs. 5 and 6) is their smallness. At $S_{or}^{wf} \approx 0.15$ one finds values in the range $10^{-4} < miCa, F < 10^{-3}$. Such values are much too small, because $miCa \ll 1$ and $F \ll 1$ would imply (viscous forces) \ll (capillary forces). But this cannot be correct, because the reduction in S_{or}^{wf} from 30% to 15% is tantamount to viscous forces being strong enough to overcome the capillary retention forces. Thus, the theory underlying the computation of $miCa$ and F deviates severely by several decades from experiment. The local macroscopic capillary number introduced above in Eq. (21) removes and unravels this discrepancy in expected and unexpected ways.

B. Computation of local macroscopic CNCs

Knowledge of velocity v_w , viscosity μ_w , and interfacial tension σ are obviously not sufficient to compute $lmCa$ from Eq. (21). In fact, σ does not appear at all in Eq. (21). The computation of local macroscopic capillary numbers, however, requires pore space parameters such as porosity ϕ and permeability k . Their values are taken from Table I. The sample length is taken to be $L = 5.08$ cm for all samples. More specific or individual core lengths were not given in [25].

The saturations S_i in Eq. (21) are set to $S_w = 1 - S_{or}^{wf}$ for $i = w$ and $S_o = S_{or}^{wf}$ for $i = o$. The value for $k_{rw}^c(S_w)$ is taken from column 7 of Table 3 in [25]. The normalized capillary pressure in Eq. (21) is computed as

$$\widehat{P}_c(S_i) = 10^{-G/\lg[(1-S_{or}-S_{ai})/(1-S_{ai})]} - 1 \quad (28)$$

using G and S_{ai} from Table I. The number 1 is subtracted to account for the fact that all water floods are imbibition processes, while Eq. (18) and the functions in Fig. 1 are for drainage. Finally P_b is computed as

$$P_b = \frac{\sigma P_d^{\text{exp}}}{P_d^{\text{th}} 10^{-G/\lg(1/2)}} \sqrt{\frac{\phi}{k}}, \quad (29)$$

where the last column in Table I is used as a correction factor for Leverett-J-function estimates.

C. Comparison of rock types

The microscopic capillary number correlations $S_{or}^{wf}(miCa)$ for Berea sandstone (sample 880) and Indiana limestone (sample 881) from Ref. [25] (Table 3) are plotted in Fig. 2. Left-pointing triangles are used for Berea sandstone, while pentagons are used for Indiana limestone. Clearly, both fall within the ranges $10^{-7} < miCa < 10^{-2}$ and $0.15 < S_{or}^{wf} < 0.40$ as in Ref. [25] (Fig. 4). Therefore, the traditional microscopic capillary number correlation $S_{or}^{wf}(miCa)$ implies the force balance in the two rocks is comparable and it is not possible to distinguish the two samples based on their capillary desaturation behavior. However, such a conclusion would be premature.

Computing the local macroscopic capillary numbers from Eq. (21) yields the correlation $S_{or}^{wf}(lmCa)$. The results for Berea sandstone are plotted as right-pointed triangles in Fig. 2 and hexagons for Indiana limestone. For both rocks one finds $lmCa > 1$, i.e., the local macroscopic capillary number agrees

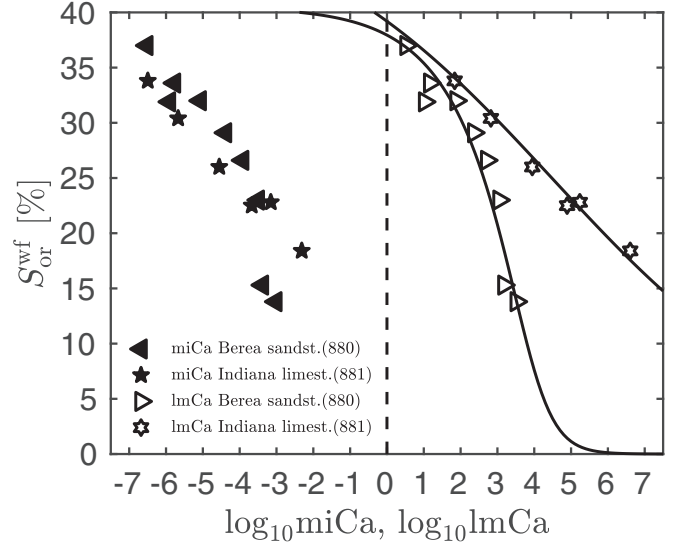


FIG. 2. Capillary number correlations $S_{or}^{wf}(miCa)$ (filled symbols) and $S_{or}^{wf}(lmCa)$ (open symbols) for Berea sandstone (sample 880) and Indiana limestone (sample 881). The vertical dashed line marks equality of viscous and capillary forces. The two solid lines are fits with Eq. (26) with parameters $S_{or}^{pl} = 40.5\%$, $A = 10^4$, $\alpha = 1$, $\beta = 0.3$ (Berea sandstone) and $S_{or}^{pl} = 50\%$, $A = 3 \times 10^4$, $\alpha = 0.125$, $\beta = 1$ (Indiana limestone).

with the experimentally observed force balance for both rocks. In all water floods the viscous forces were larger than the capillary forces. While this result might have been expected from Ref. [23] (Fig. 2), the amount by which the data are shifted has not been anticipated. The data for Berea sandstone are shifted by seven decades, while those for Indiana limestone are shifted by nine decades to the right. As a result, local macroscopic capillary number correlations clearly separate Berea sandstone (sample 880) from Indiana limestone (sample 881), a result that has been overlooked until now.

Figure 2 shows two solid lines representing interpolations of $S_{or}^{wf}(lmCa)$ using the fit function from Eq. (26). The parameters are $S_{or}^{pl} = 40.5\%$, $A = 10^4$, $\alpha = 1$, $\beta = 0.3$ for Berea sandstone and $S_{or}^{pl} = 50\%$, $A = 3 \times 10^4$, $\alpha = 0.125$, $\beta = 1$ for Indiana limestone. In limestone much larger viscous forces than in sandstone are needed to reach the same residual oil saturation. This conforms well to experience of reservoir engineers in the field. The solid line interpolations shown in Fig. 2 will be used for extrapolation in Sec. VI E below.

The difference between $S_{or}^{wf}(miCa)$ and $S_{or}^{wf}(lmCa)$ arises from the difference in the capillary pressure functions between the two samples. In this way, the local macroscopic capillary numbers reveal unexpected information that has been hidden in the data of [25], and was overlooked for 45 years. To see that the result is due to the capillary forces and not to the difference in permeability between Berea sandstone and Indiana limestone, the Berea sandstone is replaced with a Bandera sandstone having a permeability $k = 32$ md comparable to $k = 26$ md of the limestone. The pore geometrical factors of the two rocks are different. Figure 3 shows the comparison of Bandera sandstone (sample 879) against Indiana limestone (sample 881). Again the microscopic

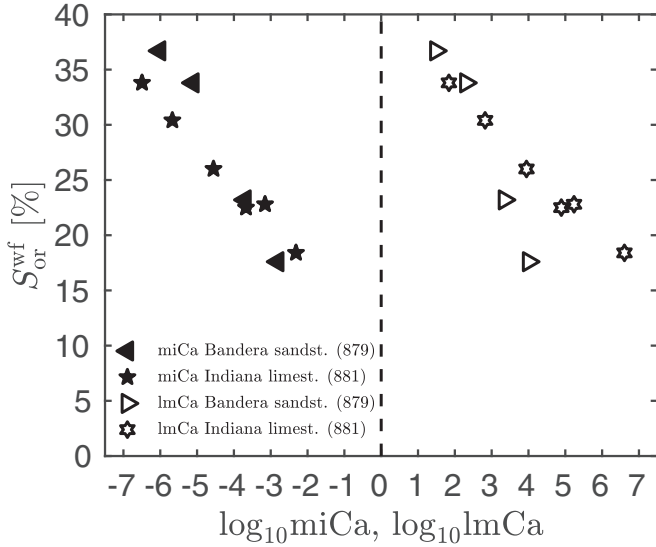


FIG. 3. Capillary number correlations $S_{or}^{wf}(\text{miCa})$ (filled symbols) and $S_{or}^{wf}(\text{lmCa})$ (open symbols) for Bandera sandstone (sample 879) and Indiana limestone (sample 881). The vertical dashed line marks equality of viscous and capillary forces.

correlation $S_{or}^{wf}(\text{miCa})$ shows overlapping or entangled datasets. The force balance changes dramatically for lmCa and one finds $\text{lmCa} > 1$ for both rocks. Plotting the local macroscopic correlation $S_{or}^{wf}(\text{lmCa})$, the datasets for the two rocks become disentangled.

Figure 4 shows a comparison between two sandstones with nearly the same porosity. The permeabilities of $k = 490$ md for Dalton sandstone (sample 798) and $k = 1860$ md for Paluxy sandstone differ by a factor ≈ 3 . The pore geometrical factors are $G = 0.1$ for Dalton and $G = 0.05$ for Paluxy. Again the overall force balance gives $\text{lmCa} > 1$ for both

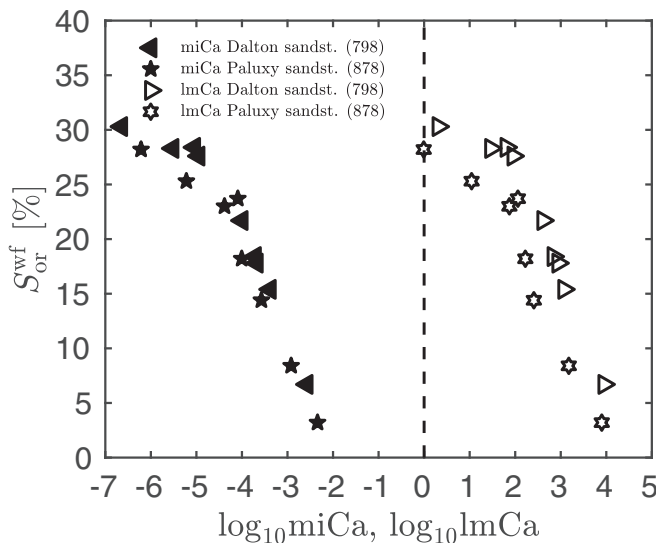


FIG. 4. Capillary number correlations $S_{or}^{wf}(\text{miCa})$ (filled symbols) and $S_{or}^{wf}(\text{lmCa})$ (open symbols) for Dalton sandstone (sample 798) and Paluxy sandstone (sample 878). The vertical dashed line marks equality of viscous and capillary forces.

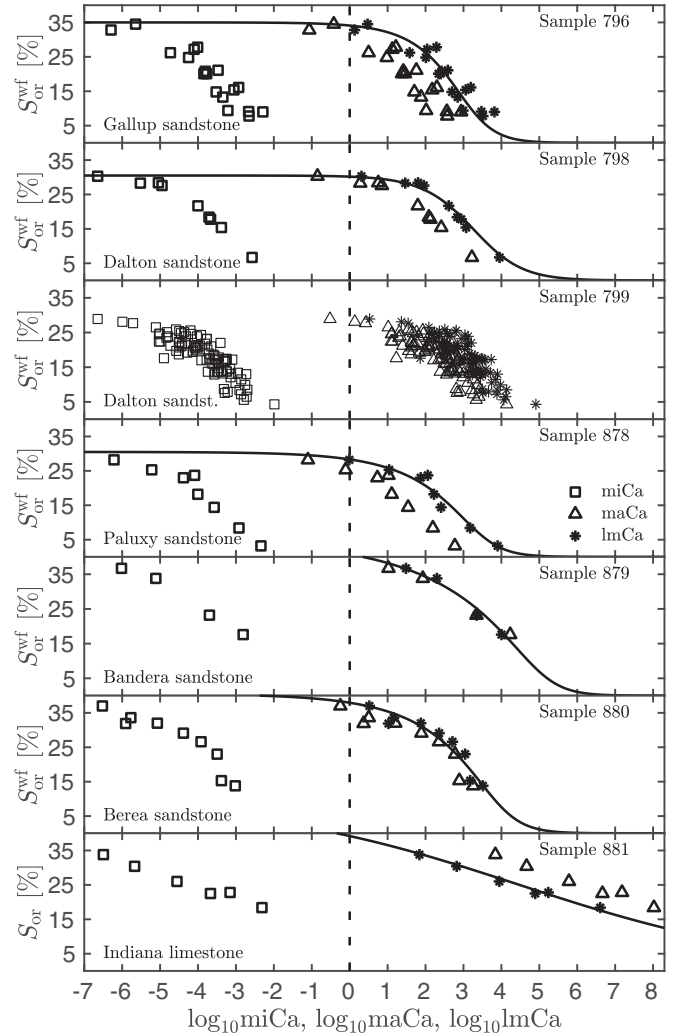


FIG. 5. Comparison of capillary number correlations $S_{or}^{wf}(\text{miCa})$ (square), $S_{or}^{wf}(\text{maCa})$ (triangle), and $S_{or}^{wf}(\text{lmCa})$ (asterisk) for all samples. The solid lines are fits to $S_{or}^{wf}(\text{lmCa})$ using Eq. (26) with fit parameters listed in Table III. The vertical dashed line marks equality between capillary and viscous forces.

rocks. In this case, the difference between the two rocks is smaller. Yet, the two rock types are clearly separated from each other in the $S_{or}^{wf}(\text{lmCa})$ -correlation, while both rocks are overlapping and indistinguishable from each other in their $S_{or}^{wf}(\text{miCa})$ -correlations.

In summary, the analysis of experimental capillary desaturation curves using local macroscopic capillary numbers lmCa allows us to differentiate between different types of rocks.

D. Comparison of CNCs

Figure 5 compares three different capillary number correlations. Each subfigure shows microscopic $S_{or}^{wf}(\text{miCa})$, macroscopic $S_{or}^{wf}(\text{maCa})$, and local macroscopic $S_{or}^{wf}(\text{lmCa})$ capillary number correlations. There is one subfigure for each of the seven samples in [25]. While the microscopic correlation $S_{or}^{wf}(\text{miCa})$ shows little or no differences between sandstone and limestone, the macroscopic correlations $S_{or}^{wf}(\text{maCa})$ and $S_{or}^{wf}(\text{lmCa})$ differentiate clearly between rock

TABLE III. Fit parameters for the local macroscopic capillary number correlations for six different rock samples using Eq. (26).

No.	Description	S_{or}^{pl}	A	α	β
796	Gallup sandstone	0.35	1500	1.0	0.5
798	Dalton sandstone	0.305	2500	0.7	0.83
878	Paluxy sandstone	0.305	3000	1.0	0.33
879	Bandera sandstone	0.45	130000	1.0	0.2
880	Berea sandstone	0.405	10000	1.0	0.3
881	Indiana limestone	0.5	30000	0.125	1.0

types. This is due to the fact that maCa and lmCa depend on the properties of the porous medium, while miCa does not.

Note that the number of different fluid pairs used for the water floods is largest for sample 799. It is to be expected that similar data clouds arise for the other samples when more fluid pairs are used. A first indication for this is seen in sample 796.

Six subfigures of Fig. 5 show a solid line fit to the $S_{or}^{wf}(lmCa)$ correlation using Eq. (26). The parameters for these fits are listed in Table III. The data cloud for sample 799 has not been fitted, because it will be analyzed in more detail in Sec. VI E.

For most of the sandstones except Bandera sandstone one sees that maCa < lmCa at given and fixed S_{or}^{wf} . For Bandera sandstone one has maCa \approx lmCa, and for Indiana limestone maCa > lmCa the inequality is reversed.

E. Extrapolations

The six interpolating fits in Fig. 5 and Table III cannot be used uncritically for extrapolations. The reason is that the fit parameters depend on the viscosity ratio and the interfacial tension of the fluid pair. This dependence was studied systematically for sample 799 in [25] and is visualized by the data cloud for sample 799 in Fig. 5.

In an attempt to study this dependence, the data for sample 799 (Dalton sandstone) were separated according to their figure of merit H . Each fluid pair has a different figure of merit H defined in Eq. (27), which can be computed from Table II. For each fixed H the data were fitted separately. The plateau saturation $S_{or}^{pl} = 0.295$ was used in all cases. Figure 6 shows such an individual fit to those data points of sample 799 that have $H = 0.167$. Figure 7 shows the fit parameters A, α, β as functions of $\lg H$. The resulting fits to all the data of sample 799 are seen in Fig. 8.

The results seem to show that the exponents α and β increase with $\lg H$. The uncertainty is significant, because for most values of H the data do not span a large enough range in S_{or}^{wf} or lmCa. With these precautions in mind the solid lines in Fig. 8 can be used to extrapolate the capillary number correlations for sample 799. It is to be expected that a similar bundle of extrapolation trajectories would be found also for the other samples. An indication for this can be seen from the data for Gallup sandstone in Fig. 5.

VII. LIMITS OF VALIDITY

As discussed above, the inequality (4) is the local condition of validity, applicability, and consistency for the constitutive

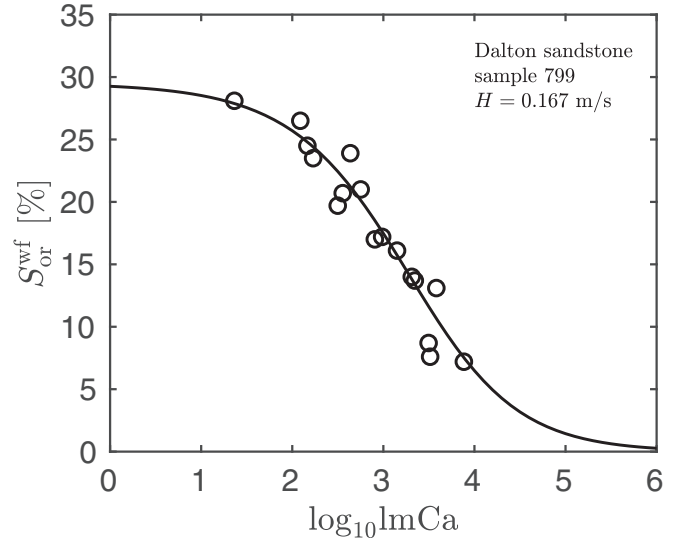


FIG. 6. An individual fit of $S_{or}^{wf}(lmCa)$ to those data for sample 799 having figure of merit $H = 0.167$ m/s.

equations (6) and (13). Demanding a force balance of less than 10^{-2} , say, one has

$$miCa_w \approx 10^{-2} \ll 1, \tag{30a}$$

$$maCa_w \approx 10^{-2} \ll 1, \tag{30b}$$

$$lmCa_w \approx 10^{-2} \ll 1 \tag{30c}$$

for the three types of capillary numbers. Then Fig. 5 shows that inequality (30a) is fulfilled for all rocks and all water floods. This would seem to indicate that the generalized Darcy theory is always applicable and consistent in all cases. However, this is not true, because as already noted above miCa depends upon the interfacial tension σ , and σ is not a material parameter in the generalized Darcy model represented by (6) and (13).

The inequalities (30b) and (30c) are never fulfilled. They contain only parameters from the generalized Darcy model (6)

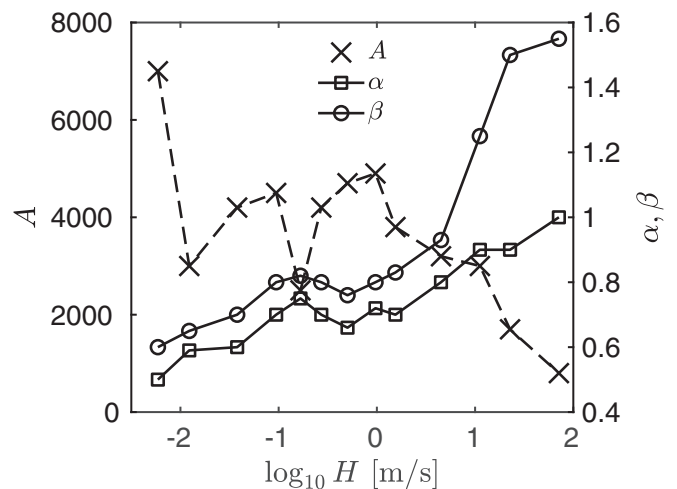


FIG. 7. Fit parameters $A, \alpha,$ and β from Eq. (26) as a function of $\lg H$, where $H = \sigma \mu_o / \mu_w^2$ is the figure of merit in Eq. (27).

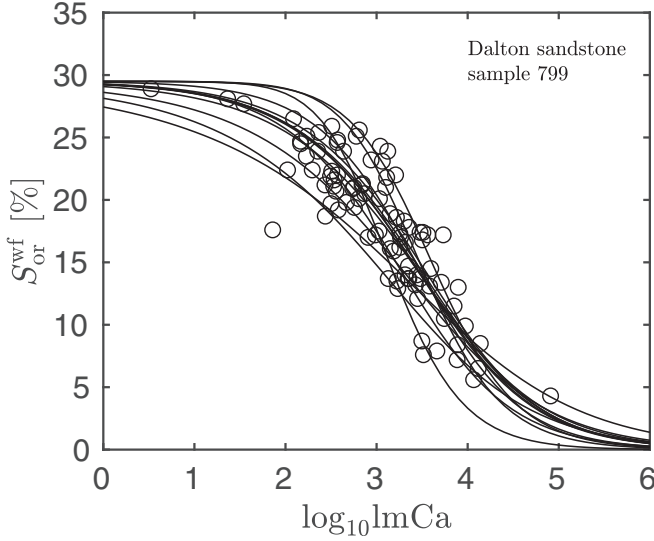


FIG. 8. All fits of local macroscopic capillary number correlations at fixed H for the data of sample 799. The plot shows one solid line for each parameter combination $A(H)$, $\alpha(H)$, $\beta(H)$ with fixed H . The parameter combinations are shown in Fig. 7. In all cases, $S_{or}^{pl} = 0.295$ is used.

and (13). Accordingly, the conditions of validity, consistency, and applicability of the generalized Darcy theory are violated for all samples and all fluid pairs in [25]. This is an important new insight that seems to have been overlooked. On the other hand, the macroscopic numbers $maCa$ and $lmCa$ conform to experimental observations and theoretical expectations in the sense that they predict theoretically a force balance ≈ 1 when experimentally mobilization of trapped oil is observed. To summarize the paradoxical situation, the successful generalized Darcy theory predicts its own inapplicability to the water floods documented in [25].

VIII. MIXED WETTABILITY

All samples discussed and analyzed above were processed to become strongly water wet [25]. The influence of wettability on residual oil saturation has been investigated for Berea sandstone in [27]. It is usually assumed that the plateau saturation for the wetting phase lies below that for the nonwetting phase, and that the critical capillary number for the wetting phase is larger than for the nonwetting phase (Ref. [28], Fig. 3-17).

To define mixed wettability macroscopically, let $P_c(S)$ denote the capillary pressure function for an immiscible displacement process (e.g., a water flood) in some sample. Let S_z denote a zero of this function, $P_c(S_z) = 0$, and assume that no other zeros exist. The sample is called strongly water wet if $P_c(S) \geq 0$ for all $S_{wi} < S \leq S_z$ and $S_z \approx 1 - S_{or}$. It is called strongly oil wet if $P_c(S) \geq 0$ for all $S_{wi} < S \leq S_z$ and $S_z \approx S_{wi}$. A sample is called mixed wet if it is neither strongly water wet nor strongly oil wet.

Having defined wettability macroscopically, a problem for extending the present analysis emerges clearly. For oil

wet samples one has $P_b < 0$ for $S_z < (S_{wi} + 1 - S_{or})/2$ and hence $maCa < 0$. The problem is solved by using the absolute value $|P_c|$ instead of P_c . For mixed wet cores one has $P_b \approx 0$ when $S_z \approx (S_{wi} + 1 - S_{or})/2$. This would (incorrectly) seem to indicate that capillary forces are small or absent.

One way to address this problem is to observe that a water flood starting from an initial oil saturation near S_{wi} is an imbibition process for $S_{wi} < S < S_z$. It becomes a drainage process for $S_z < S < 1 - S_{or}$. An oil flood is an imbibition process for $S_z < S < 1 - S_{or}$ and a drainage process for $S_{wi} < S < S_z$. This suggests to extend Eq. (17) as

$$P_b = \begin{cases} P_c \left(\frac{S_{wi} + S_z}{2} \right) & \text{for } S_z \geq \frac{S_{wi} + 1 - S_{or}}{2}, \\ |P_c \left(\frac{S_z + 1 - S_{or}}{2} \right)| & \text{for } S_z < \frac{S_{wi} + 1 - S_{or}}{2} \end{cases} \quad (31)$$

to mixed wettability.

IX. CONCLUSIONS

Analysis of the experiments in [25] supports the following conclusions:

(1) Microscopic capillary number correlations $S_{or}^{wf}(miCa)$ are qualitatively misleading, because $miCa$ depends only on fluid properties, but not on properties of the porous medium.

(2) Microscopic capillary number correlations $S_{or}^{wf}(miCa)$ are quantitatively misleading, because $miCa \ll 1$ in theory when viscous forces clearly dominate capillary forces in experiment.

(3) Macroscopic capillary number correlations $S_{or}^{wf}(maCa)$ depend on geometry and wetting properties of the porous medium through P_b , k , and ϕ .

(4) Macroscopic capillary numbers $maCa$ fulfill $maCa \approx 1$ when viscous forces overcome capillary forces.

(5) Macroscopic capillary number correlations $S_{or}^{wf}(maCa)$ depend on length scale.

(6) Mercury porosimetry data can be used to estimate oil-water capillary pressure functions when the samples are strongly water wet.

(7) Local macroscopic capillary number correlations $S_{or}^{wf}(lmCa)$, introduced in Eq. (21), seem to quantify the balance between viscous and capillary forces even better than $S_{or}^{wf}(maCa)$.

(8) Viscous forces influence $lmCa$ through $k^r(S)$, which is not the case for $maCa$.

(9) The difference between rocks enters into $lmCa$ and $maCa$ through P_b , k , ϕ and the constitutive functions k^r and P_c .

(10) A fit function has been introduced in Eq. (26). It contains three parameters and is asymmetric.

(11) A figure of merit H has been introduced that correlates well with the parameters of local macroscopic capillary number correlations for sample 799 in [25].

(12) The exponents α , β in Eq. (26) seem to be increasing functions of the figure of merit.

ACKNOWLEDGMENTS

The author thanks Dr. Hu Guo for discussions and the Deutsche Forschungsgemeinschaft for financial support.

-
- [1] L. Kadanoff, *J. Stat. Phys.* **39**, 267 (1985).
[2] P. de Gennes, *Europhys. Lett.* **5**, 689 (1988).
[3] R. Lenormand, E. Touboul, and C. Zarcone, *J. Fluid Mech.* **189**, 165 (1988).
[4] T. Delker, D. B. Pengra, and P. Z. Wong, *Phys. Rev. Lett.* **76**, 2902 (1996).
[5] A. Scheidegger, *The Physics of Flow Through Porous Media* (University of Toronto Press, Toronto, 1957).
[6] J. Bear, *Dynamics of Fluids in Porous Media* (Elsevier, New York, 1972).
[7] D. Green and G. Willhite, *Enhanced Oil Recovery* (Society of Petroleum Engineers, Richardson, 2018).
[8] S. Broadbent and J. Hammersley, *Math. Proc. Cambridge Philos. Soc.* **53**, 629 (1957).
[9] S. Kirkpatrick, *Rev. Mod. Phys.* **45**, 574 (1973).
[10] J. Essam, *Rep. Prog. Phys.* **43**, 833 (1980).
[11] D. Stauffer and A. Aharony, *Introduction to Percolation Theory* (Taylor and Francis, London, 1992).
[12] Z. Liu, J. E. McClure, and R. T. Armstrong, *Phys. Rev. E* **98**, 043102 (2018).
[13] P. A. Gago, P. King, and A. Muggeridge, *Phys. Rev. Appl.* **10**, 034003 (2018).
[14] R. T. Armstrong, J. E. McClure, M. A. Berrill, M. Rucker, S. Schlüter, and S. Berg, *Phys. Rev. E* **94**, 043113 (2016).
[15] Q. Lin, B. Bijeljic, S. Berg, R. Pini, M. J. Blunt, and S. Krevor, *Phys. Rev. E* **99**, 063105 (2019).
[16] F. Dullien, *Porous Media—Fluid Transport and Pore Structure* (Academic, San Diego, 1992).
[17] R. Schneider and W. Weil, *Stochastische Geometrie* (Teubner, Stuttgart, 2000).
[18] M. Muskat, *The Flow of Homogeneous Fluids through Porous Media* (McGraw-Hill, New York, 1937).
[19] R. Hilfer, *J. Math. Phys.* **59**, 103511 (2018).
[20] H. Rabbani, D. Or, Y. Liu, C.-Y. Lai, N. Lu, S. Datta, H. Stone, and N. Shokri, *Proc. Natl. Acad. Sci. (USA)* **115**, 4833 (2018).
[21] R. Hilfer, *Adv. Chem. Phys.* **92**, 299 (1996).
[22] G. Willhite, *Waterflooding*, SPE Textbook Series Vol. 3 (Society of Petroleum Engineers, USA, 1986).
[23] L. Anton and R. Hilfer, *Phys. Rev. E* **59**, 6819 (1999).
[24] J. Thomeer, *J. Petro. Tech.* **12**, 73 (1960).
[25] A. Abrams, *Soc. Pet. Eng. J.* **15**, 437 (1975).
[26] R. Hilfer and P. Øren, *Transp. Porous Media* **22**, 53 (1996).
[27] K. Humphry, B. Suijkerbuijk, H. van der Linde, S. Pieterse, and S. Masalmeh, Impact of wettability on residual oil saturation and capillary desaturation curves (2013), paper SCA2013-025.
[28] L. Lake, *Enhanced Oil Recovery* (Prentice Hall, Englewood Cliffs, NJ, 1989).